Research Article

Journal of Environmental Nanotechnology

Tribological Optimization of Al/ZrO_2 Nanocomposites: Influence of Reinforcement Content on Wear Performance Using Taguchi Method

T. Shaafi[1], M. Kalaimani[1*], M. Yuvaperiyasamy[1], Krishna Prakash Arunachalam[2] and M. Karthigairajan[3]

[1]Department of Mechanical Engineering, Saveetha School of Engineering, Saveetha Institute of Medical and Technical Sciences (SIMATS), Chennai, TN, India

[2]Departamento de Ciencias de la Construcción, Facultad de Ciencias de la Construcción Ordenamiento Territorial, Universidad Tecnológica Metropolitana, Santiago, Chile

[3]Department of Mechanical Engineering, Karpaga Vinayaga College of Engineering and Technology, Chengalpattu, TN, India

Received: 15.05.2025 Accepted: 18.06.2025 Published: 30.06.2025

*mkalaikvn@gmil.com

ABSTRACT

This study investigates the tribological behaviour of aluminium matrix nanocomposites reinforced with Zirconium dioxide (ZrO_2) nanoparticles, synthesized using the powder metallurgy method. Three different compositions were prepared: AlZ3 (3 wt.% ZrO_2), AlZ6 (6 wt.% ZrO_2), and AlZ9 (9 wt.% ZrO_2), with aluminium as the base matrix. The mechanical mixing was performed using a high-energy ball mill, followed by compaction and sintering in a controlled environment. Wear performance was evaluated using a pin-on-disk tribometer under varying loads and sliding distances. The Taguchi method using an L_9 orthogonal array was employed to design the experiments and determine the optimal combination of normal applied load (NAL), sliding distance (SD), and ZrO_2 content for minimizing wear rate, friction coefficient, and specific wear. Additionally, the ANOVA method was employed to identify the key factors influencing wear resistance and to evaluate the significance of their effects. Regression analysis is used to model and predict the relationship between process parameters and better wear resistance. It quantifies the influence of each factor, enabling accurate optimization of conditions for improved wear performance. Taguchi analysis reveals that the optimal conditions are a normal applied load of 30N, sliding distance of 1000 m and 6 wt.% of ZrO_2 nano reinforcement. The R^2 values for wear rate 84.58%, friction factor 87.79%, and specific wear 81.51% indicate strong model fits. These results confirm that the regression models effectively capture the variability in wear performance metrics.

Keywords: Zirconium dioxide; Wear resistance; Design of experiments; Analysis of variance; Aluminium nanocomposite.

1. INTRODUCTION

Aluminium metal matrix composite (AMMC) is a remarkable composite of lightweight qualities, durability, corrosion resistance, and improved mechanical strength; aluminum matrix composites (AMCs) are often used in many industries, including automotive, aerospace, marine, and electronics (Kar *et al.* 2024). The aluminum composite has more attention to improve their properties of the mechanical, wear resistance, corrosion resistance, thermal stability, and prevent the chemical reaction. Many researchers focused on improving the properties above by incorporating ceramic particles in the reinforcement process (Khazin *et al.* 2022). These ceramic particles are silicon carbide (SiC)(Nie *et al.* 2025), aluminum oxide (Al_2O_3)(Wu *et al.* 2024), titanium oxide (TiO_2)(Vignesh *et al.* 2024), boron carbide (B_4C)(Babu *et al.* 2024), zirconium dioxide (ZrO_2)(Wang *et al.* 2024), and silicon nitrate (Si_3N_4)(Manghnani *et al.* 2021). These ceramic particles exhibit different properties when reinforced with an aluminium matrix; these tailoring processes were used to develop the aluminium composite for the required application (Messer *et al.* 2024). Among these ceramic particles, the ZrO_2 exhibits excellent hardness to make a high mechanical attribute and good wear resistance property that make it suitable for structural and tribological applications. These qualities of high hardness, high fracture toughness, and transformation toughening mechanism enable ZrO_2 to withstand material loss brought on by mechanical contact and friction, hence making it more wear-resistant in comparison to many other ceramics (Kumar and Irfan, 2021). Aluminium matrix composites reinforced with nanoparticles show much better tribological and mechanical properties than their microscale ceramic reinforcement equivalents (Geng *et al.*, 2018). Especially for high performance and advanced technical processes, nano-reinforced aluminium composite stands out with reduced friction coefficients, greater surface hardness, and better load-bearing capacity(Singhal *et al.* 2025). The nanoparticles included in the nanocomposite help to improve material behaviour, such as remarkable hardness, tensile strength, wear resistance, and thermal

stability (Prakash *et al.* 2024). The enhanced ratio of surface area to volume in the nanoparticles, which promotes enhanced load transmission efficiency and better-improved contact between the reinforcement and aluminium matrix, is a major cause behind these improved characteristics. Under mechanical and thermal stress, this improved microstructural interaction is essential for increasing the general performance, dependability, and lifetime of the composite (Said *et al.* 2024).

Generally, the aluminium metal matrix composite is manufactured in different states as followed by liquid state, solid state and two states (Sharma *et al.* 2021). Many researchers are focusing on fabricating the aluminium composite in different techniques, especially the aluminium nanocomposite, which is more precise to manufacture by the advanced manufacturing technique (Pooja *et al.* 2025). A comprehensive investigation of nanoparticle reinforcements and their abilities to tackle the significant difficulties of particle agglomeration, reinforcement distribution, interfacial, and structural stability is a crucial attempt that must be addressed in order to enhance the reinforcing capability of Al matrix nanocomposites (Singh *et al.* 2021). To produce alumina matrix composites, the powder metallurgy technique (PMT), in combination with various sintering processes, has proven to be a practical and cost-effective mode of operation. Controlling the particle distribution of reinforcement is a primary objective that this technology has the potential to do (Mu *et al.* 2021). The powder metallurgy (PM) procedures are among the most exciting methods because they have the potential to produce nanopowders that are both homogenous and well-dispersed. During the process of nanocomposite preparation, alloying is an intriguing approach in PM that has the potential to produce homogenized nanoparticles (Taha *et al.* 2022). Sabbar *et al.* (2021) fabricating the aluminium nanocomposite synthesis by hot extrusion and ZrO_2 nanoparticle effects are summarized and addressed. To better include metal alloys like AA7075-ZrO_2, this evaluation emphasizes thermal processing and equal channel angular pressing. AA7075-ZrO_2 was stated to be excellent for making drone components, military equipment, and other prospective applications because of its lightweight and outstanding performance. (Pal *et al.* 2020) investigated the aluminium nanocomposite in Al and ZrO_2 phases occurs independently, and ZrO_2 intensity increases with concentration. Al-ZrO_2 MMNCs with 6 wt% ZrO_2 in the Al matrix exhibit a 9.57% increase in maximum hardness and a 63.91% increase in wear resistance. The nanocomposites with the greatest 6 wt% of ZrO_2 exhibit corrosion resistance efficiency of 70%, compared to 35.55% and 41.20% for 2 wt% and 4 wt%, respectively.

Sabari *et al.* (2024) Examine the Friction Stir Welding (FSW), which is a key solid-state joining process that yields high-quality welds with high levels of mechanical properties. The reinforcement by Titanium Carbide nanoparticles (TiCnp) of AZ31 magnesium alloy welds is investigated in this study. An integrated approach involving Artificial Neural Network (ANN) and Grey Relational Analysis is used to optimize the procedure (Haja *et al.* 2022). Results indicated considerable improvement in tensile strength, microhardness and impact strength, as well as a reduction in the rate of wear. Friction Stir Welding (FSW) is an emerging solid-state joining process arising from the requirement for better mechanical performances and weld qualities. This article examines the impact of Titanium Carbide nanoparticles (TiCnp) on the AZ31 magnesium alloy welds via Grey Relational Coefficient optimization. Optimal parameters, 1250 rpm rotational speed, 50 mm/min traverse speed, 1° tilt angle and square tool profile passively enhance the weld strength. The addition of TiCnp increases tensile strength to 230 MPa with enhanced microhardness, impact strength and decreased wear rate (Sabari *et al.* 2024).

Friction Stir Processing (FSP)-reinforced hybrid metal matrix composites with graphite (Gr) and zirconia (ZrO_2) particles are examined for microstructural development, tribological characteristics, and corrosion behaviour. The pin-on-disk test showed that particle-reinforced composites had better wear resistance than base metal (BM), but FSP-treated samples had worse wear resistance. The lubricant effect of Gr particles significantly reduced the coefficient of friction (COF) and weight loss in Gr-containing composites, with the hybrid composite and Gr-reinforced mono-composite experiencing COF reductions of ~0.52 and ~0.37, respectively (Keshavarz *et al.* 2023). Experimental investigation of stir casting produced zirconia (ZrO_2) particle-filled composites with AA8011-5, AA8011-10, and AA8011-15 weight percentages (Vinoth *et al.* 2022). A Taguchi coupled TOPSIS technique predicted composite rate of wear (WR) and coefficient of friction (COF). Experimental results showed that reinforcement content contributed 55.06% to WR and COF, followed by applied load and sliding velocity at 26.32% and 12.84%, respectively. The worn composite surfaces were examined using SEM. (Manikandan *et al.* 2023) estimate the wear rate and friction of ZrO_2-filled Al 8014 matrix composites. Composite samples with 5, 10, and 15% wt ZrO_2 particle additions were stir cast. ANOVA showed that weight % of ZrO_2 content had the second-largest effect on specific wear rate and coefficient of friction after load. Develop a neural network model to anticipate replies. This model predicts the outcome with 99.78% accuracy. (P *et al.* 2022) examine the mechanical and wear properties of ultrasonic-assisted stir-cast graphene and zirconium dioxide-reinforced aluminium alloy 6061 hybrid nanocomposites. ANN and ANFIS models predicted wear rates for experimental and non-experimented parameters. Prediction analysis helped analyze composite wear. Comparing ANN and ANFIS showed that ANFIS predicted with 99.9% R^2 accuracy.

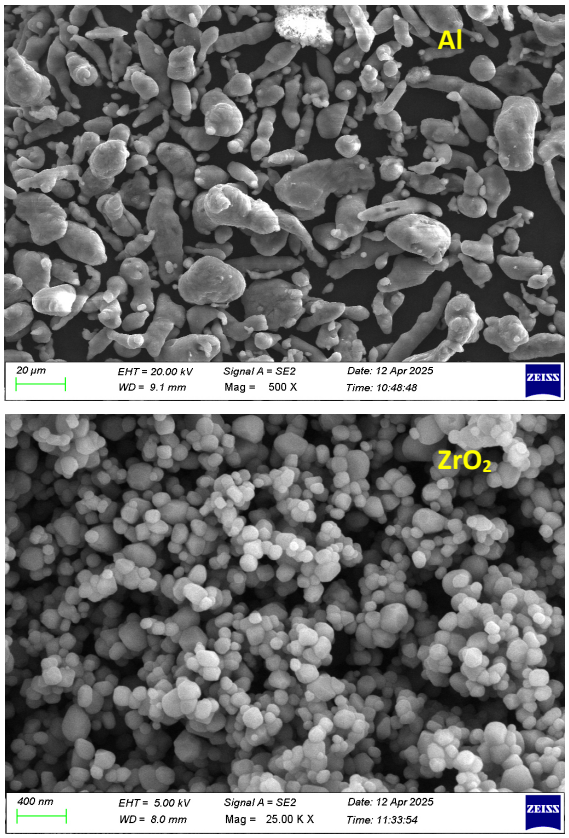


Fig. 1: (Al) Aluminum powder, (ZrO_2) Zirconium dioxide nanoparticles

This research focused on investigating the wear resistance property of Al/ZrO_2 nanocomposite. The addition of the zirconia dioxide nanoparticles significantly enhances wear resistance due to their inherent high hardness, excellent chemical stability, and changed into toughness mechanism, which improves crack resistance under mechanical stress. The ZrO_2 nanoparticles enable uniform dispersion within the aluminium matrix, enabling effective load transfer and reducing local stress concentrations. These attributes make ZrO_2 a highly suitable reinforcement for applications that require high durability under sliding wear resistance conditions. The aluminium reinforced with ZrO_2 nanoparticles leads to exhibits the improvement of maximum wear resistance, with the best result achieved within an optimal reinforcement range. While many studies have explored wear behaviour, limited research has addressed the route. Notably, the use of powder metallurgy for producing Al/ZrO_2 nanocomposite and optimizing their wear performance remains understudied. This study addresses the gap by fabricating Al/ZrO_2 nanocomposite using the PM process, which permits precise control by determining the most effective reinforcement range. Systematic assessment of the influence of many factors on wear performance was done using the Taguchi design of experiments. Statistical identification of the most important variables affecting wear behaviour was done using analysis of variance (ANOVA). The result of this work offers the best composition and process conditions to get the highest wear resistance. Additionally, the study helps to create high-performance aluminium matrix composites strengthened with ZrO_2 for innovative use in engineering.

2. MATERIALS AND METHODS

2.1 Materials

For this study, aluminium (Al) powder with a purity of 99.0% and a density of 2.7 g/cm³, APS is 20 to 40 µm selected as the base matrix powder, as indicated in Table 1. zirconium dioxide (ZrO_2), exhibiting purity of 99.0%, a density of 5.68 g/cm³, and a particle size range of 30 to 50 nm shows in Figure 1, was sourced from VEDAYUKT INDIA PVT. LTD., situated in Ghatshila, Jamshedpur, Jharkhand, India.

Table 1. Shows the composition of the nanocomposite for the specified sample

Samples Name	Al %	ZrO_2 %
AlZ3	97	3
AlZ6	94	6
AlZ9	91	9

2.2 Experimental Method

The nanocomposite sample powders were made using the composition followed by given in Table 1. A high-energy VB Ceramic Planetary ball mill was used to mix every batch for five hours. Using 10 mm diameter steel balls as the grinding medium, the milling drum ran at a steady 300 rpm. To guarantee efficient milling and particle refining, a ball-to-powder weight ratio of 5:1 was maintained. A cooling period was added every 10 minutes, following the approach described in the reference, to avoid overheating during milling. The combined powders were compacted into cylindrical billets 10 mm in diameter and 30 mm in height after milling. A hydraulic press with a load cell was utilized to deliver a compaction pressure of up to 600 MPa. A die lubricant was zinc stearate to lower punch-die friction during compaction. The thorough criteria of the powder materials and the planetary milling system. The sintering process was held in the tubular furnace at 550 °C for 180 minutes and followed by the compacted green samples are shown in Figure 2. To avoid oxidation of the aluminium matrix and zirconia reinforcement, the sintering process was carried out in a regulated environment. The samples were kept within the furnace temperature at 550 °C to drop down to room temperature after the sintering time slowly. The slow cooling of aluminium nanocomposite after the sintering process has

benefits such as minimising residual stress, preventing cracks and warping, improving microstructure stability, improving bonding strength and reducing oxidation risk.

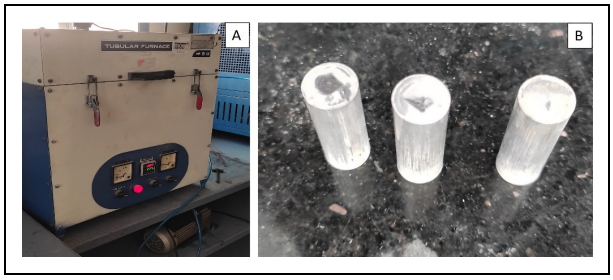


Fig. 2: (a) Tubular Furnace (b) Al/ZrO_2 nanocomposite samples

2.3 Material Testing

Zeiss, Ultra Plus performed Scanning Electron Microscope. Energy-dispersive X-ray (EDX) spectroscopy studies are conducted in the SEM on individual specimens to ascertain the chemical composition of the stated hybrid composites. XRD (X-ray diffraction) examination of the aluminium nanocomposite samples PANalytical was done with a step size of 0.02° noted in the 2θ range of 20–100°.

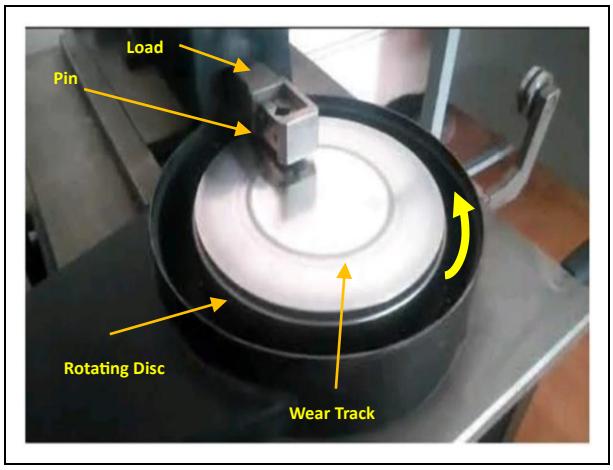


Fig. 3: Pin-on-disc wear test setup

2.4 Wear Experiment

A pin-on-disk test was performed by a Ducom Pin-on-Disc apparatus (Model No. TR-201 CL, Bangalore, India) with an accuracy of 0.1 mg. The rotating disc material was EN 32 steel, with a diameter of 120 mm and 10 mm in thickness. The wear test setup, as shown in Figure 3, was the nanocomposite sample pins with an 8 mm diameter and 25 mm length. These pins were pressed against the rotating disc against some variations of applied loads, as specified in Table 2. The configuration was utilized to understand the wear property of the composite material under controlled sliding conditions.

3. TAGUCHI METHOD DESIGN OF EXPERIMENTS

The Taguchi Method is a powerful statistical approach to optimizing product and process quality through a structured Design of Experiments (DoE) using orthogonal arrays to study multiple variables with a minimal number of experiments (Ramesh *et al.* 2024). It emphasizes making systems robust against variations (noise) by identifying optimal factor levels that enhance performance consistency and quality. A key innovation in the Taguchi method is the Signal-to-Noise (S/N) ratio, which measures the stability of a process by comparing the desired signal (mean performance) to the undesired noise (variability) (Bennett *et al.* 2025). There are three types of S/N ratio equations used depending on the objective:

For smaller-the-Better, the S/N ratio is $\frac{S}{N} = -10\log_{10}\left(\frac{1}{n}\sum y_i^2\right)$ ... (1)

Larger-the-Better, it is $\frac{S}{N} = -10\log_{10}\left(\frac{1}{n}\sum\frac{1}{y_i^2}\right)$ and ... (2)

For Nominal-the-Best, it is $\frac{S}{N} = 10\log_{10}\left(\frac{\bar{y}^2}{s^2}\right)$ ... (3)

Where y_i are the observations, $\bar{y}$ is the mean, s is the standard deviation, and n is the No. of trails. By maximizing the S/N ratio, the method ensures high-quality output that remains stable under varying real-world conditions, making it highly effective across fields like manufacturing, automotive, electronics, and healthcare (Tran *et al.*, 2024).

Table 2. L_9 orthogonal array and their levels

S. No.	Factors	Low	Medium	High
1	Normal applied load (NAL) (N)	10	30	50
2	Sliding distance (SD) (m)	500	1000	1500
3	wt.% ZrO_2	3	6	9

3.1 Analysis of Variance

ANOVA (Analysis of Variance) is a statistical method used to assess whether there are significant differences between the means of three or more independent groups by partitioning total variation in a dataset into components attributed to different sources (Gajević *et al.* 2024). It separates the total variability into between-group variance, which reflects differences among group means, and within-group variance, which represents natural variability within each group. The

technique calculates an F-statistic by taking the ratio of between-group variance to within-group variance (Rafiei and Ghasemi, 2024). A large F-value, accompanied by a p-value below a predefined significance level (commonly 0.05), leads to the rejection of the null hypothesis, suggesting that there is a statistically significant difference among at least one group mean. ANOVA serves as a fundamental tool in experimental design, quality control, and scientific research for identifying influential factors and optimizing processes (Sahoo *et al.* 2024).

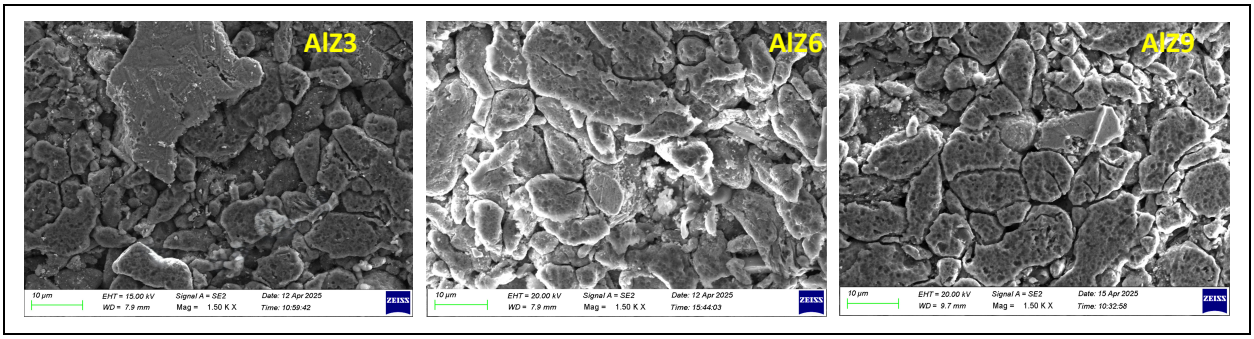


Fig. 4: SEM of nanocomposite samples, (AlZ3) 3wt.% of ZrO_2, (AlZ6) 6wt.% of ZrO_2, (AlZ9) 9wt.% of ZrO_2

4. MATERIALS CHARACTERIZATION

4.1 SEM Image of Aluminum Nano Composite Samples

The SEM images reveal that Aluminum nanocomposites that were reinforced with different weight fractions of ZrO_2 nano ceramic particles such as a sample AlZ3, AlZ6 and AlZ9 at the weight percentages of 3 wt%, 6 wt% and 9 wt% respectively. This rise in ZrO_2 nano concentration is confirmed by characteristic scanning electron micrographs exhibiting the grain shape and particle interaction with the matrix, as shown in Figure 4. The grains in AlZ3 have a coarse structure with well-bounded surfaces, and the distribution of ZrO_2 nanoparticles is limited, which implies less interaction between the reinforcement and the aluminium matrix. The SEM image of the AlZ6 sample, which contains 6 wt% ZrO_2, shows a very tight and polished grain structure. Within the matrix, the white fields indicating ZrO_2 nano ceramic particles are more clearly visible and densely packed. Though some level of agglomeration is suspected from the increased particle loading, the matrix particle surfaces are clearly defined. The SEM study reveals no apparent voids or interfacial fractures, hence suggesting good wettability and metallurgical bonding. The total grain refinement is significant; consistent with the grain boundary pinning effect, the area percentage of reinforcement increases with increasing ZrO_2 concentration. This microstructural behaviour verifies that when the reinforcement % rises, the interfacial bonding improves, grain size lowers, and the structural integrity of the nanocomposite is strengthened. The trend shown confirms the anticipated increase in mechanical and wear resistance characteristics resulting from enhanced dispersion and interface strength. The AlZ9 sample SEM micrographs reveal a clear grain size refinement and a more uniform and denser distribution of ZrO_2 nanoparticles over the aluminium matrix as the ZrO_2 nano concentration rises to 9 wt% in. Reflecting better adhesion between the matrix and nano reinforcements, the aluminium matrix interface seems cleaner and more coherent. With several different nanoceramic particles buried within the matrix, the reinforcement visibility also increases. A more consistent microstructure results from this better distribution and bonding, which is expected to increase the mechanical performance and load transmission capacity of the composite.

4.2 EDX Study of Aluminum Nanocomposite Samples

Confirming the elemental composition and the effective integration of ZrO_2 nano reinforcement into the aluminium matrix, Figure 5 shows the Energy Dispersive X-ray Spectroscopy (EDX) study of the Al/xZrO_2 (x = 3, 6, and 9 wt.%) nanocomposites. The EDX spectrum of AlZ3 confirms the inclusion of ZrO_2 nanoparticles in trace but purposeful amounts by showing the predominant presence of aluminium at 91.89 wt%, along with oxygen (6.52 wt%) and zirconium (1.59 wt%). The AlZ6 composite has 89.88 wt% aluminium, a little drop from the AlZ6 composite; zirconium is constant at 1.6 wt%, and oxygen rises somewhat to 8.52 wt%. AlZ9 shows an especially greater oxygen peak at 15.19 wt%, suggesting more ceramic reinforcing content; aluminium falls to 83.25 wt% while zirconium stays fairly steady at 1.56 wt%. The rising oxygen level across the samples reflects the gradual addition of ZrO_2 nanoparticles, which are very oxygen-rich by mass. Zirconium value consistency and increasing oxygen levels confirm the uniform dispersion of ZrO_2 nanoparticles within the matrix. The spectra show no superfluous components or contaminants, hence confirming the purity of the manufactured nanocomposites. The findings also point to

adequate bonding and dispersion of ZrO_2 within the aluminium matrix as the reinforcement % rises, which is essential for improving the thermal and mechanical characteristics of the composite materials.

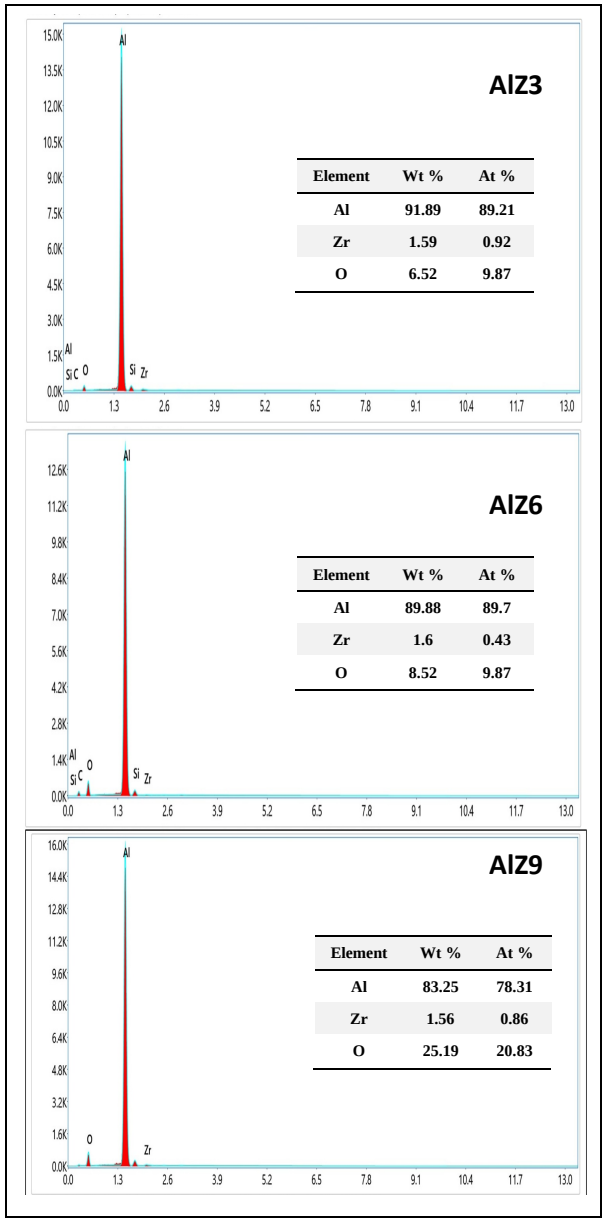


Fig. 5: EDX study of nanocomposite samples, (AlZ3) 3wt.% of ZrO_2, (AlZ6) 6wt.% of ZrO_2, (AlZ9) 9wt.% of ZrO_2

4.3 XRD Analysis of Aluminum Nanocomposite Samples

Figure 6 is the XRD patterns of Al/ZrO_2 nanocomposites having different ZrO_2 reinforcement levels of 3 wt% (AlZ3), 6 wt% (AlZ6) and 9 wt% (AlZ9) confirming the formation of Al-based metal matrix nanocomposites (MMNCs). The diffraction peaks reveal the face-centred cubic (FCC) structure of the aluminium matrix of typical reflection from the (111), (200), (220), (311), and (222) planes, based on standard JCPDS card no: 89-4037 (Şenel *et al.* 2019), for pure aluminium. The correspond to the monoclinic or tetragonal phases of ZrO_2, in particular at low values: around 28-33° and 50-55°, clearly confirm the existence of zirconia in the standard of JCPDS card no. 37–1484 (Pal *et al.* 2020). The lack of additional peaks of impurity confirms the extraordinary purification level of the aluminium matrix and ZrO_2 nano reinforcements. In particular, the intensity of the ZrO_2 peaks increases gradually depending on ZrO_2 concentration in AlZ6 and AlZ9 samples indicating the successful inclusion and an increased phase fraction of ZrO_2 in these composites. Higher ZrO_2 nano contents exhibit negligible peak broadening on the primary Al peaks, and these are due to the lattice strains and smaller crystallite sizes. This decrease in the size of crystallite is more influential in AlZ9 since higher pinning of the ZrO_2 nanoparticles on the grain boundaries is implied. The major Al peaks are relatively unchanged, which indicates that ZrO_2 nanoparticles are the different phases and not the solid solutions with the Al matrix. Increasing reinforcement peak intensity and diminishing Al peak sharpness indicate increased strengthening and refining of grains by increased amount of ZrO_2 rise. Such results further validate the existence of the structural integrity and phase composition as regards the Al/ZrO_2 nanocomposites, whereby the reinforcement concentration directly influences the resulting composites' crystalline structure and dispersion quality.

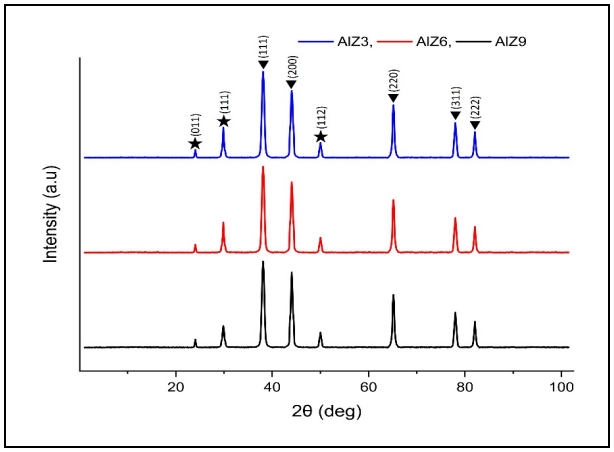


Fig. 6: XRD analysis of nanocomposite samples, (AlZ3) 3wt.% of ZrO_2, (AlZ6) 6wt.% of ZrO_2, (AlZ9) 9wt.% of ZrO_2

5. RESULT AND DISCUSSION

The experimental observations were analyzed using the Taguchi method, which is a systematic and statistical approach to optimize process parameters by studying the effect of multiple variables through a minimal number of experiments. In this study, the factors considered were NAL, SD, and the weightage % of ZrO_2 reinforcement, each varied at three levels. An L_9 orthogonal array is used, and the interactions among these input responses were assessed based on the output responses—wear rate, friction factor, and specific wear

rate. Since all these responses are undesirable and need to be minimized, the "smaller-the-better" signal-to-noise (S/N) ratio criterion was utilized to ascertain the optimal settings. It was observed that lower applied loads resulted in reduced wear and friction due to decreased contact stress and thermal generation at the sliding interface. At higher loads, the material experienced more severe surface interactions and deformation, leading to increased wear. The sliding distance had a variable impact depending on the reinforcement level; longer sliding distances tend to increase wear, but this effect was mitigated when higher ZrO_2 content was used. The reinforcement with ZrO_2 played a significant role in enhancing the tribological performance. A higher %age of ZrO_2 improved the material's hardness, load-bearing capacity, and resistance to surface damage. The ceramic particles acted as a barrier against plastic deformation and helped maintain the integrity of the material surface under sliding conditions.

Among the different parameter combinations, the best tribological performance was observed under the optimal conditions of applied load, sliding distance, and ZrO_2 content. This combination created favourable conditions by minimizing mechanical stress and enhancing surface protection through the reinforcing effect of ZrO_2 particles is examined. A higher percentage of reinforcement enhanced the hardness of the material and resistance to deformation, effectively reducing wear and friction. In contrast, applying higher loads with lower reinforcement levels resulted in greater surface damage and material degradation. The Taguchi analysis demonstrated the wear behaviour is significantly affected by the interplay of load factors, sliding distance, and reinforcement content, and careful optimization of these parameters is crucial for enhancing wear resistance and overall tribological performance. The results of the experiments conducted using the Taguchi Method are shown in Table 3.

Table 3. Experimental observation by the Taguchi method

S. No.	Normal Applied Load (N)	Sliding Distance (m)	wt.% ZrO_2	Wear Rate (mm^3/m)	Friction Factor	Specific Wear (mm^3/m)
1	10	500	3	0.0072896	3.0365	0.0003569
2	10	1000	6	0.0244896	8.6780	0.0014578
3	10	1500	9	0.0032537	3.1120	0.0002269
4	30	500	6	0.0113588	12.6780	0.0016685
5	30	1000	9	0.0123568	8.8960	0.0050012
6	30	1500	3	0.0188660	6.1245	0.0013215
7	50	500	9	0.0106365	4.2354	0.0005514
8	50	1000	3	0.0088365	7.9256	0.0004589
9	50	1500	6	0.0167737	3.8765	0.0011665

Table 4. Response table for wear rate

Level	Normal Applied Load (N)	Sliding Distance (m)	wt.% ZrO_2
1	41.57	40.37	39.44
2	37.18	37.15	35.54
3	38.68	39.92	42.46
Delta	4.39	3.22	6.92
Rank	2	3	1

Table 4 illustrates the response table for wear rate, highlighting the influence of three variables: NAL (N), SD (m), and wt.% ZrO_2 at three distinct levels. The table provides the wear rate values for each factor at its respective levels, where Level 1 displays the wear rate for NAL (41.57 N), sliding distance (40.37 m), and wt.% ZrO_2 (39.44), with a reduction in wear rate observed at Level 2 (37.18 N, 37.15 m, 35.54 wt.% ZrO_2) and Level 3 (38.68 N, 39.92 m, 42.46 wt.% ZrO_2). The Delta values represent the difference between the highest and lowest wear rate values for each factor, with the most significant variation observed in wt.% ZrO_2 (6.92), followed by NAL (4.39 N) and SD (3.22 m). The Rank values indicate the relative significance of each factor in affecting wear rate, with wt.% ZrO_2 having the most significant impact (Rank 1), followed by normal applied load (Rank 2), and sliding distance (Rank 3). Figure 7 presents the mean signal-to-noise (S/N) ratios for the wear rate based on three factors: NAL (N), SD (m), and wt.% ZrO_2. The plot demonstrates how the S/N ratio is influenced by each factor at different levels. For NAL (N), the S/N ratio shows a decreasing trend as the load increases, indicating that lower applied loads yield a more favourable wear rate. Similarly, for SD (m), the S/N ratio decreases with an increase in sliding distance, implying that shorter distances result in better wear performance. In contrast, for wt.% ZrO_2, the S/N ratio increases as the ZrO_2 content rises, suggesting that higher levels of ZrO_2 contribute to

improved wear resistance. The optimal conditions for minimizing the wear rate are a normal applied load of 30N, sliding distance of 1000 m and wt.% ZrO_2 of 6%.

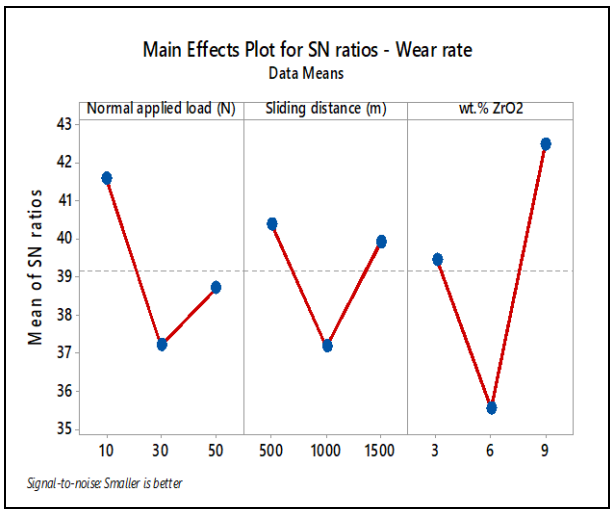


Fig. 7: Mean S/N ratio for wear rate

Table 5 presents the friction factor response values across three variables: NAL (N), SD (m), and wt.% ZrO_2, each measured at three different levels. At Level 2, the friction factor increases for all three factors, with NAL at -18.93, SD at -18.58, and wt.% ZrO_2 at -17.53. At Level 3, the friction factor decreases to -14.10 for applied load, -12.46 for SD, and -13.79 for wt.% ZrO_2. The Delta values, showing the variation range for each factor, are 6.17 for applied load, 6.12 for SD, and 3.74 for ZrO_2. The Rank values highlight the importance of each factor, with normal applied load (Rank 1) having the greatest influence on the friction factor, followed by sliding distance (Rank 2) and wt.% ZrO_2 (Rank 3).

Table 5. Response table for friction factor

Level	Normal Applied Load (N)	Sliding Distance (m)	wt.% ZrO_2
1	-12.76	-14.75	-14.46
2	-18.93	-18.58	-17.53
3	-14.10	-12.46	-13.79
Delta	6.17	6.12	3.74
Rank	1	2	3

Figure 8 illustrates the Main Effects Plot for the Signal to Noise (S/N) ratios of the friction factor, highlighting the influence of three factors NAL, SD, and wt% ZrO_2 on friction performance. The plot shows that as the NAL increases, the S/N ratio decreases, indicating better friction performance at lower applied loads. Similarly, the S/N ratio decreases with increased sliding distance, suggesting that shorter sliding distances enhance friction behaviour. In contrast, the S/N ratio increases with higher wt. % ZrO_2, indicating that higher ZrO_2 content improves the friction factor. The optimal settings for minimizing the friction factor are achieved with an applied load of 30N and SD of 1000m, along with 6 wt.% of ZrO_2.

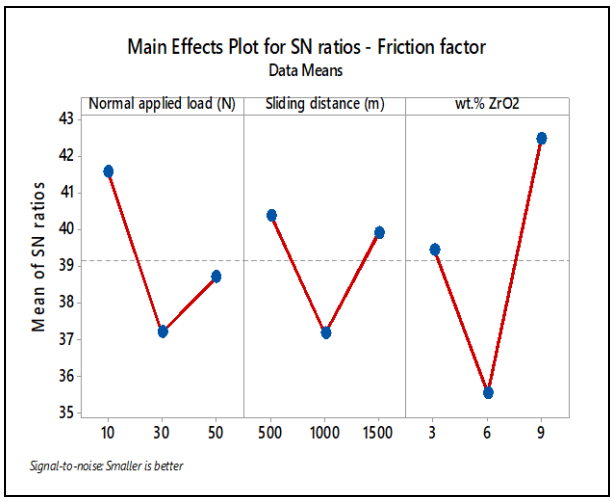


Fig. 8: Mean S/N ratio for Friction factor

Table 6 presents the response data for specific wear, showing the effect of three factors: NAL, SD, and wt. % ZrO_2 across three levels. At Level 1, the specific wear values are 70.25 for NAL, 60.07 for SD, and 63.14 for wt. % ZrO_2. At Level 2, the specific wear decreases to 50.06 for NAL, 63.67 for SD, and 64.77 for wt. % ZrO_2. At Level 3, the specific wear increases again, with values of 69.78 for NAL, 66.35 for SD, and 62.18 for wt. % ZrO_2. The Delta values represent the range of variation for each factor, with NAL showing the largest variation at 20.19, followed by SD at 6.28, and wt. % ZrO_2 at 2.60. The Rank values indicate the relative significance of each factor on specific wear, with NAL having the greatest impact (Rank 1), followed by SD (Rank 2), and wt. % ZrO_2 (Rank 3).

Table 6. Response table for specific wear

Level	Normal Applied Load (N)	Sliding Distance (m)	wt.% ZrO_2
1	70.25	60.07	63.14
2	50.06	63.67	64.77
3	69.78	66.35	62.18
Delta	20.19	6.28	2.60
Rank	1	2	3

Figure 9 presents the Main Effects Plot for the Signal to Noise (S/N) ratios of specific wear, depicting the effect of three factors: NAL, SD, and wt. % ZrO_2. The plot reveals that as the NAL increases, the S/N ratio decreases, indicating that lower applied loads are more favourable for minimizing specific wear. Similarly, as the SD increases, the S/N ratio also decreases, suggesting that shorter sliding distances contribute to reduced wear. In contrast, the S/N ratio increases with higher wt. %

ZrO_2, showing that higher concentrations of ZrO_2 improve specific wear performance. These trends demonstrate that the optimal settings for minimizing specific wear involve NAL of 30N and SD of 1000m, combined with 6 wt. % of ZrO_2.

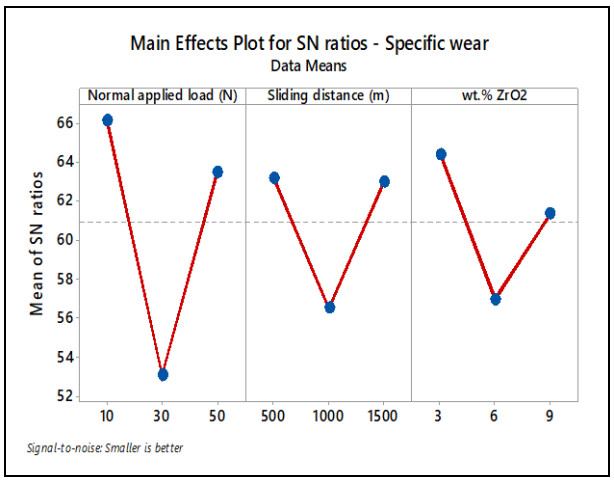


Fig. 9: Mean S/N ratio for specific wear

Figures 7, 8, and 9 present the interaction plots for wear rate, friction factor, and specific wear, respectively. The interaction plot for wear rate, as shown in Figure 10, demonstrates the combined effects of NAL, SD, and wt. % ZrO_2 on wear rate. The plot reveals that increasing the NAL results in a higher wear rate, with a more pronounced effect at higher SD, as evidenced by the steep slopes in the interaction graphs. For SD, the wear rate increases with higher distances at lower applied loads, but this trend becomes less pronounced as the applied load increases.

Additionally, the wt. % ZrO_2 exhibits a strong interaction with both NAL and SD, where higher ZrO_2 content results in a reduction in wear rate, particularly at higher applied loads and sliding distances. These interactions indicate that wear rate is significantly influenced by the combination of these factors, with wt. % ZrO_2 plays a key role in reducing wear under specific conditions.

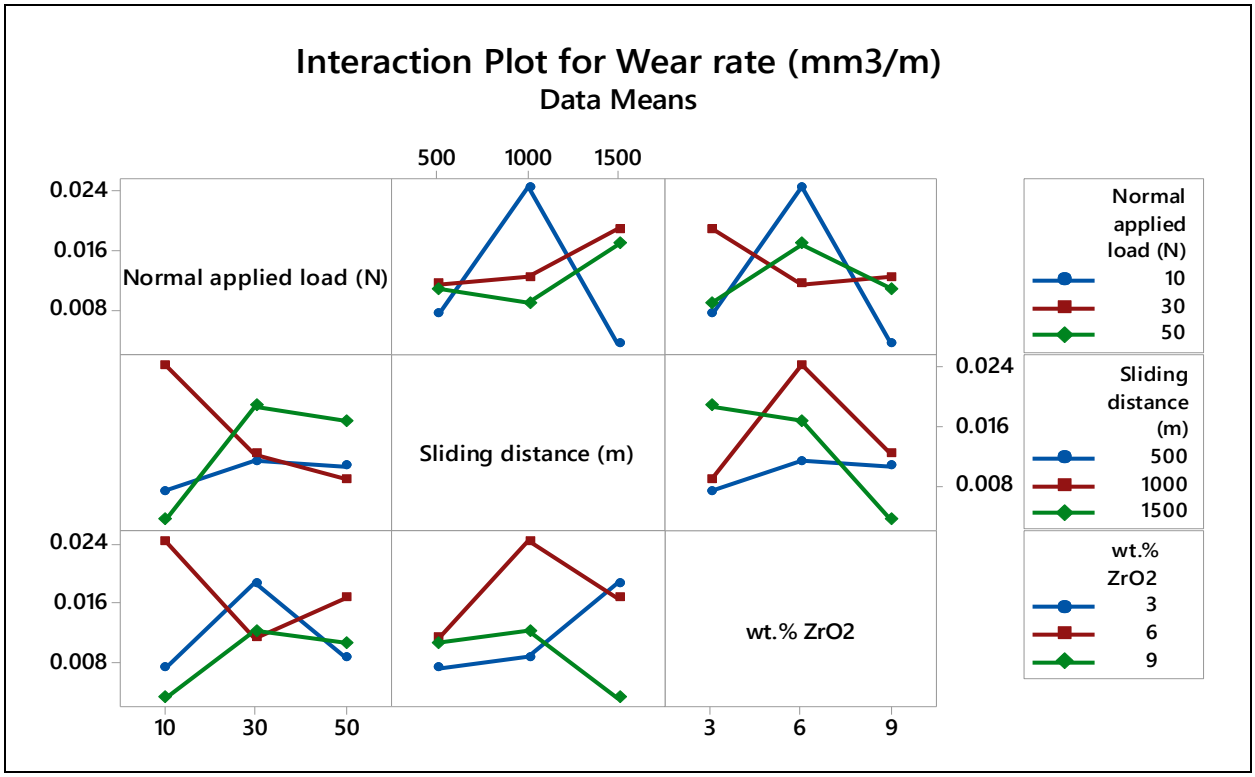


Fig. 10: Interaction plot for wear rate

The interaction plot for the friction factor as depicted in Figure 11 illustrates the effects of NAL, SD, and wt. % ZrO_2 on friction behavior. It shows that as NAL increases, the friction factor also increases, with the highest increase observed at longer sliding distances, particularly at higher levels of NAL. This indicates a strong dependence on friction on load, especially under increased SD. In contrast, sliding distance itself shows an inverse relationship with the friction factor at lower loads, but the trend becomes less pronounced as the load increases. The wt. % ZrO_2 affects the friction factor in a way that higher ZrO_2 concentrations reduce friction,

particularly at higher applied loads and longer sliding distances. These interactions highlight that both the applied load and ZrO_2 content play significant roles in determining friction behaviour, with the optimal levels leading to reduced friction under certain conditions.

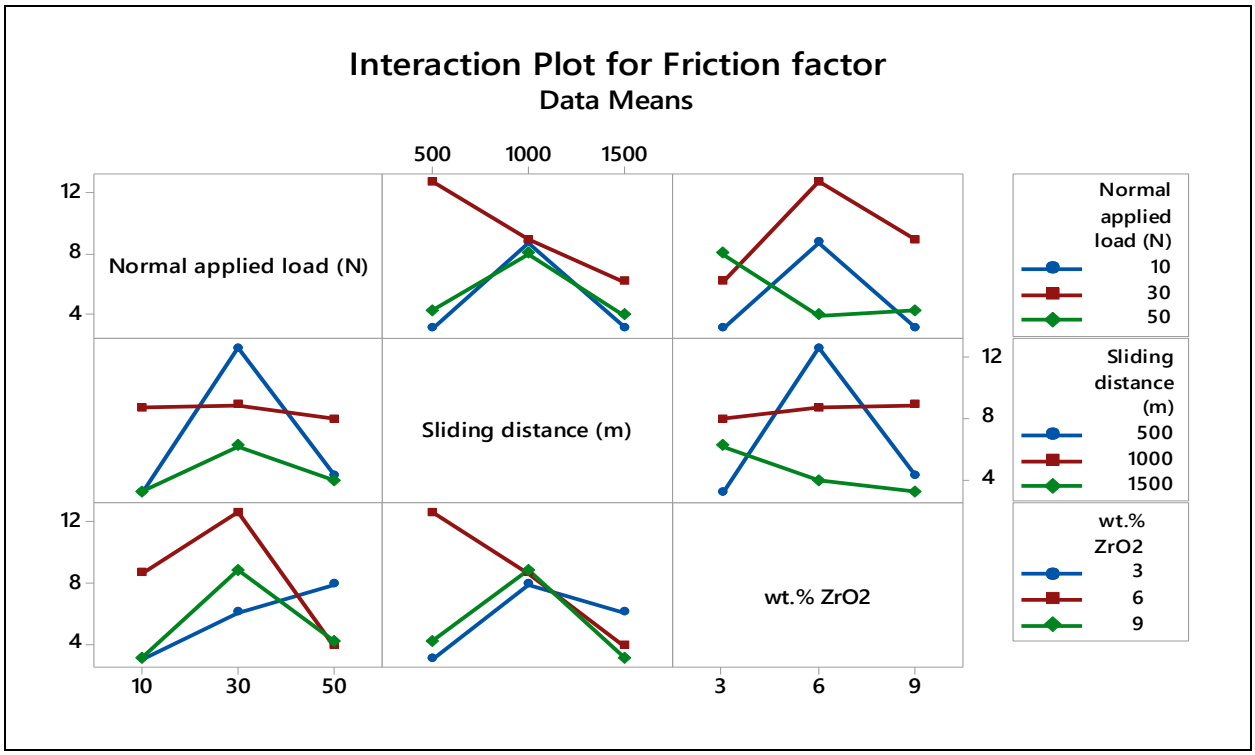


Fig. 11: Interaction plot for friction factor

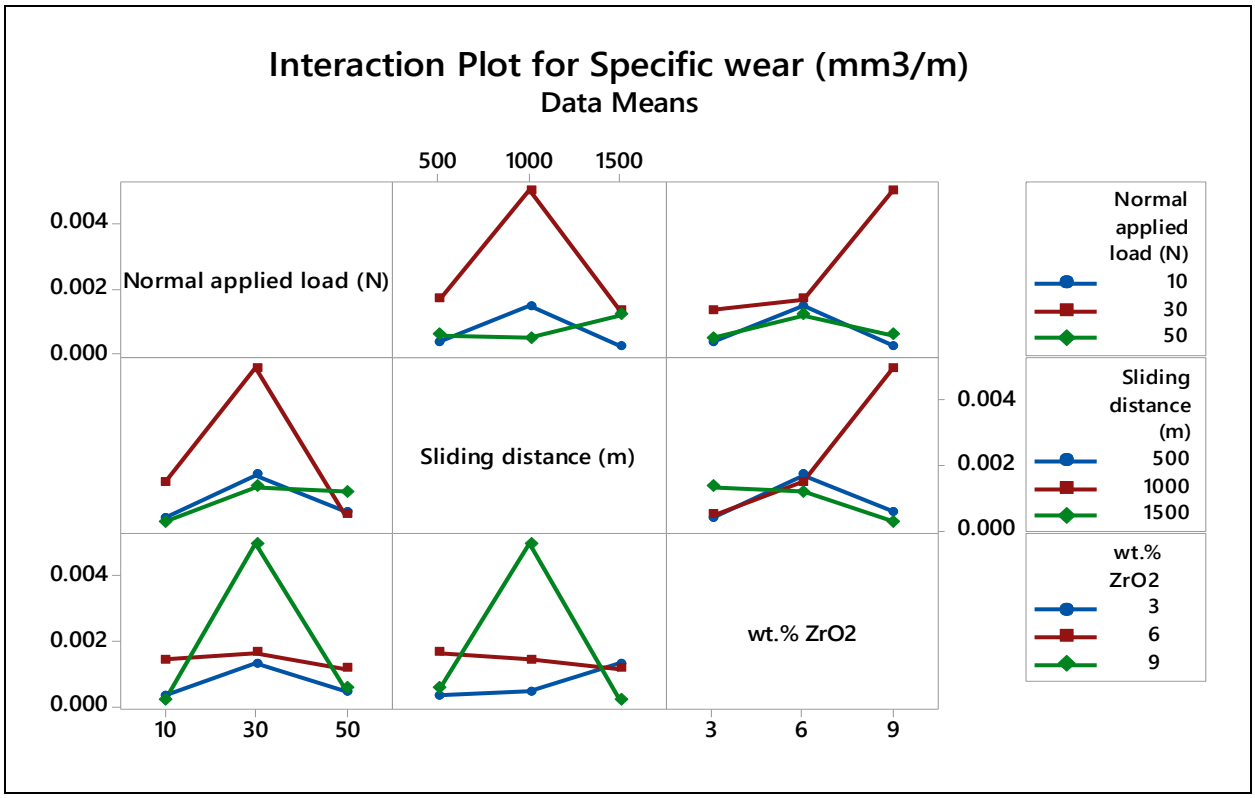


Fig. 12: Interaction plot for specific wear

The interaction plot for specific wear presented in Figure 12 shows the combined effects of NAL, SD, and wt. % ZrO_2 on particular wear. The graph demonstrates that as NAL increases, specific wear also increases, particularly at higher SD, indicating a significant interaction between these two factors. Additionally, sliding distance exhibits a similar trend, where specific wear increases with longer distances, especially under higher applied loads. The wt. % ZrO_2 has an apparent effect on reducing specific wear, particularly at higher applied loads and longer SD. The interaction plots reveal that increasing ZrO_2 content helps reduce specific wear across various load and distance conditions, suggesting that higher ZrO_2 concentrations provide better wear resistance under specific operational conditions.

Table 7 shows the ANOVA results for wear rate, indicating the contributions of NAL, SD, and wt. % ZrO_2. The normal applied load has a minimal effect with a p-value of 0.935 while sliding distance (p-value 0.776) and wt. % ZrO_2 (p-value 0.566) also show no significant impact. The error term contributes 3.30%, and the total variation is distributed as 47.15% for NAL, 13.51% for SD, and 36.04% for wt. % ZrO_2.

Table 7. ANOVA for wear rate

Source	DF	Adj SS	Adj MS	F-Value	P-Value	% Contribution
Normal applied load (N)	2	0.000120	0.000060	0.77	0.566	36.04
Sliding distance (m)	2	0.000045	0.000023	0.29	0.776	13.51
wt.% ZrO_2	2	0.000157	0.000005	0.07	0.935	47.15
Error	2	0.000011	0.000078			3.30
Total	8	0.000333				100.00

Table 8 shows the ANOVA results for friction factor, with NAL contributing 39.02%, SD 29.73%, and wt. % ZrO_2 19.04% to the total variation. Despite these contributions, the p-values (0.238 for NAL, 0.291 for Sd, and 0.391 for wt. % ZrO_2) indicate that none of the factors have a statistically significant effect on friction factor. The error term contributes 12.21% to the total variation.

Table 8. ANOVA for friction factor

Source	DF	Adj SS	Adj MS	F-Value	P-Value	% Contribution
Normal applied load (N)	2	33.68	16.841	3.20	0.238	39.02
Sliding distance (m)	2	25.66	12.832	2.44	0.291	29.73
wt.% ZrO_2	2	16.43	8.215	1.56	0.391	19.04
Error	2	10.54	5.268			12.21
Total	8	86.31				100

Table 9 presents the ANOVA for specific wear, showing that NAL contributes 47.06%, SD 23.53%, and wt. % ZrO_2 17.65% to the total variation. Despite these contributions, the p-values (0.292 for normal applied load, 0.439 for SD, and 0.587 for wt. % ZrO_2) indicate that none of the factors have a statistically significant effect on specific wear. The error term accounts for 11.76% of the total variation.

Table 9. ANOVA for specific wear

Source	DF	Adj SS	Adj MS	F-Value	P-Value	% Contribution
Normal applied load (N)	2	0.000008	0.000004	2.42	0.292	47.06
Sliding distance (m)	2	0.000004	0.000002	1.28	0.439	23.53
wt.% ZrO_2	2	0.000003	0.000001	0.70	0.587	17.65
Error	2	0.000002	0.000002			11.76
Total	8	0.000017				100.00

In this study, linear regression modeling was applied using Minitab 17.0 software to create predictive mathematical models for compressive strength and water absorption, based on selected input variables. The data maintained consistency throughout the analysis. The resulting models are expressed in the following equations: Eq. (4) for wear rate, Eq. (5) for friction factor, and Eq. (6) for specific wear.

$$\text{Wear rate } (mm^3/m) = 0.0121 + 0.000010 \text{ Normal applied load (N)} + 0.000003 \text{ Sliding distance (m)} - 0.00049 \text{ wt.\% } ZrO_2 \quad \ldots (4)$$

$$\text{Friction factor (N)} = 8.76 + 0.0101 \text{ Normal applied load (N)} - 0.00228 \text{ Sliding distance (m)} - 0.047 \text{ wt.\% } ZrO_2 \quad \ldots (5)$$

$$\text{Specific wear } (mm^3/m) = 0.00006 + 0.000001 \text{ Normal applied load (N)} + 0.000000 \text{ Sliding distance (m)} + 0.000202 \text{ wt.\% } ZrO_2 \quad \ldots (6)$$

The R^2 values for wear rate, friction factor, and specific wear are 84.58%, 87.79%, and 81.51%, respectively. An R^2 value close to 1 signifies an excellent fit of the model to the data, suggesting that these models explain a significant portion of the variability in the results. Figures 13, 14, and 15 display the residual plots for wear rate, friction factor, and specific wear, respectively, providing insights into the model's fit and the distribution of errors for each response. The residual plots for wear rate, friction factor, and specific wear provide insights into the accuracy and fit of the models for each response. In the Normal Probability Plot, all three graphs show that the residuals follow a near-normal distribution, indicating that the assumptions of normality for the model errors are met. In the Versus Fits Plot, the residuals are scattered randomly around the zero line for each response, suggesting that the model fits the data well without any clear patterns, which implies that the model is appropriate for the data. The Histogram plots show a symmetrical distribution of residuals for all three responses, further supporting the assumption of normality. In the Versus Order Plot, residuals show no clear trend or structure across observations, indicating that the errors are random and not influenced by the order of data collection, confirming that there is no autocorrelation in the residuals. These plots suggest that the models for wear rate, friction factor, and specific wear provide a good fit to the data without significant deviations from assumptions.

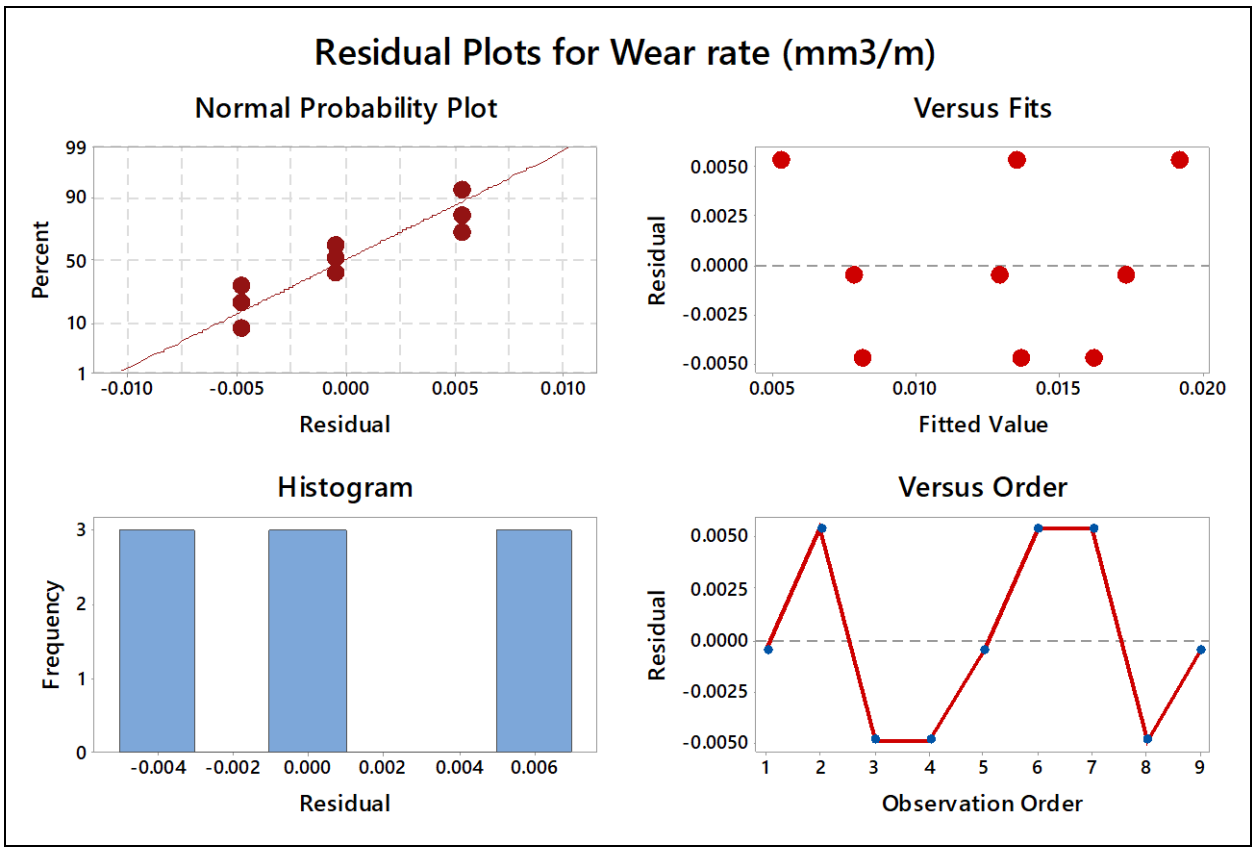


Fig. 13: Residual plots for wear rate

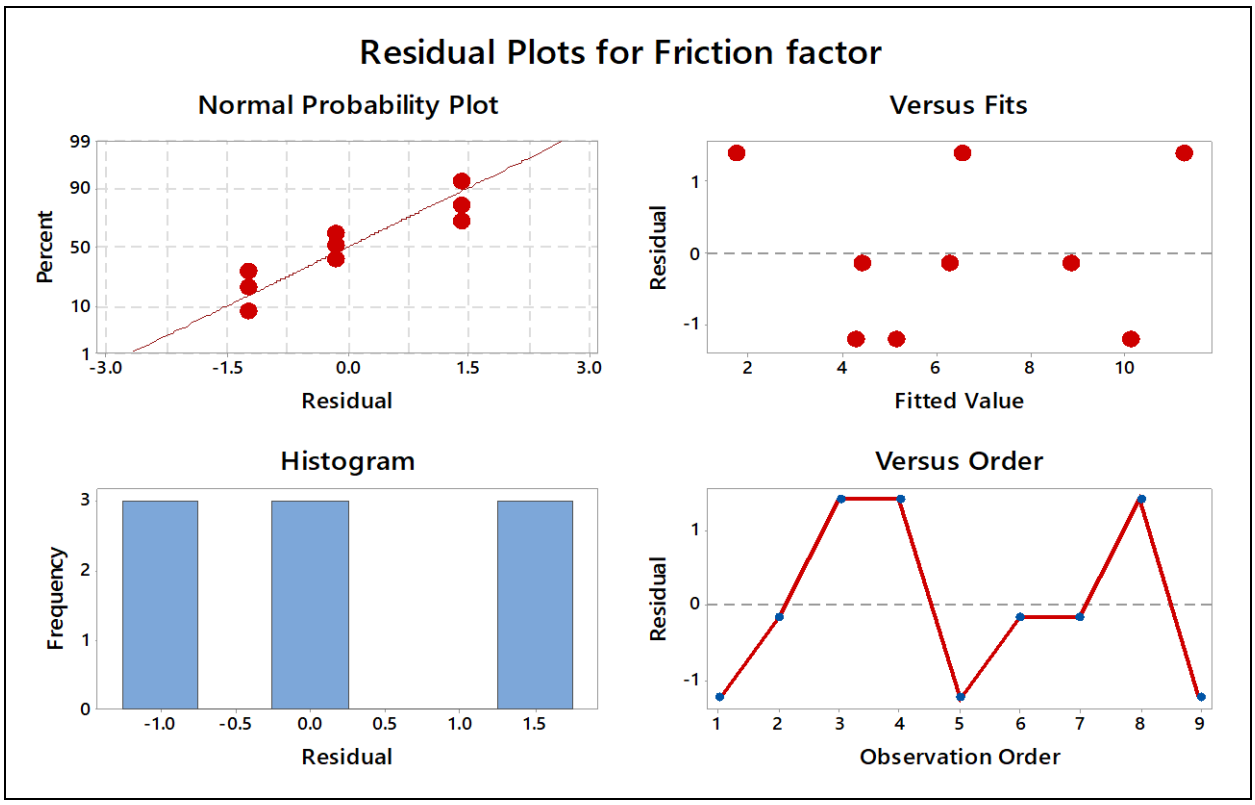


Fig. 14: Residual plots for friction factor

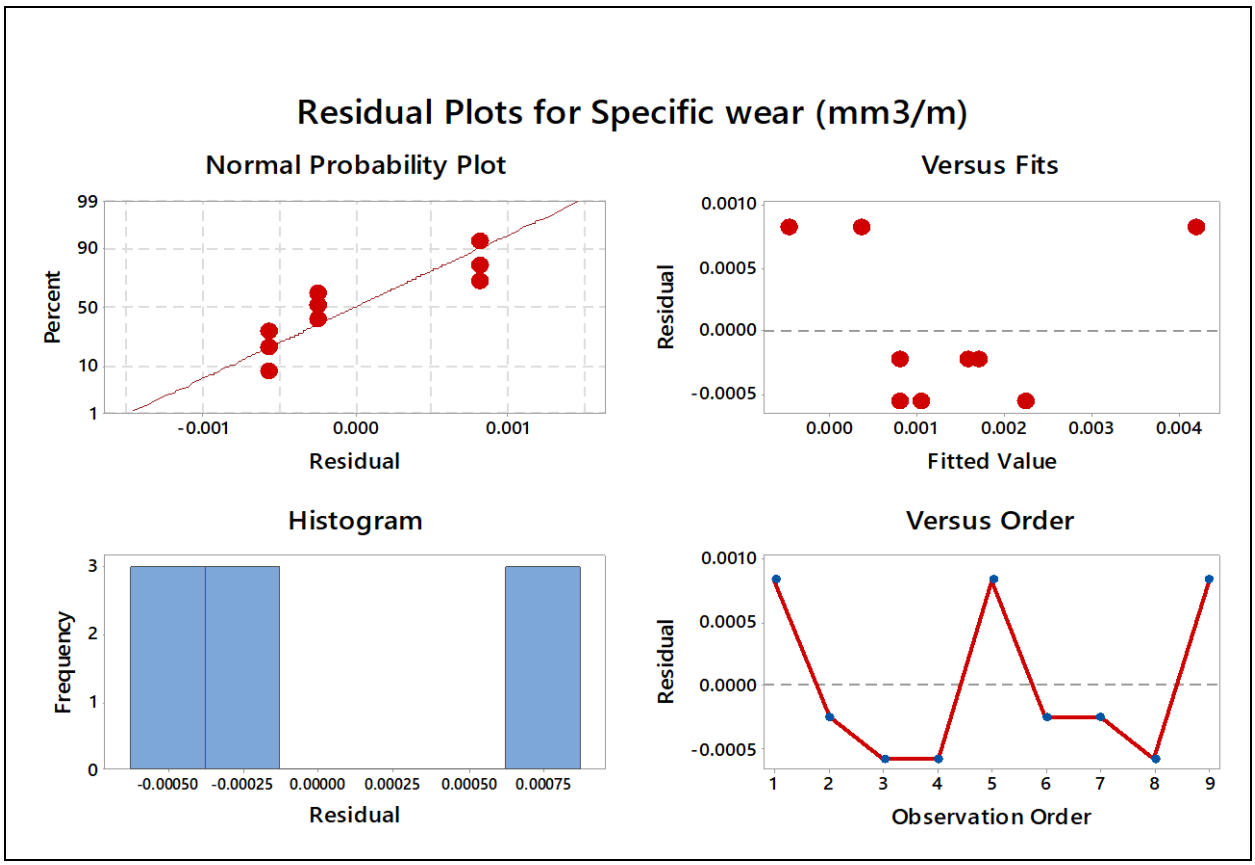


Fig. 15: Residual plots for specific wear

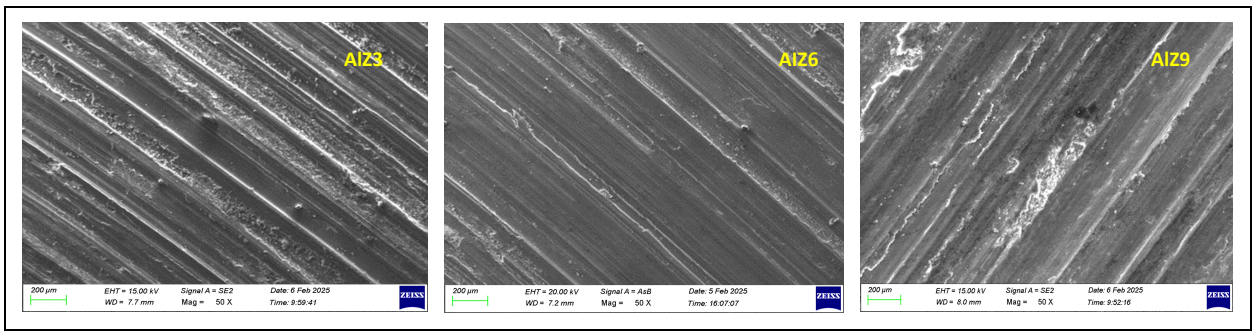


Fig. 16: Worn-out surface of nanocomposite samples

The worn sliding surface of Al Z3 (3 wt.% ZrO_2) surface showed deep continuous grooves in the direction of sliding, which is indicative of dominant adhesive wear and plastic deformation. Slight reinforcement obtained from the relatively low ZrO_2 content enabled easy deformation of the soft aluminium under applied loads. Particulate debris could be seen, suggesting the material had detached during sliding. In contrast, AlZ6 (6 wt.% ZrO_2) showed a smoother surface with finer and more uniform grooves, which suggests better wear resistance. Increased ceramic content improved surface hardness and the carrying capacity of loads, reducing material loss and surface damage. AlZ6 had lower debris formation and less noisy wear features, making it the most stable of the three samples, as shown in Figure 16. However, the AlZ9 (9 wt. % ZrO_2) sample evidenced a rougher surface with evidence for delamination, particle pullout, and micro cracks. High ZrO_2 content resulted in brittle behaviour and potential particle agglomeration upon which weak zones were developed during sliding. This led to an enhanced abrasive and delamination wear even though it was of high hardness. Overall, AlZ6 performed the best with the best wear properties because of its proper combination of hardness and toughness.

6. CONCLUSION

The results from the experimental and optimization studies are as follows:

The optimal conditions for minimizing the wear rate, friction factor, and specific wear are a normal applied load of 30 N, a sliding distance of 1000 m, and wt.% ZrO_2 of 6%.

Analysis of variance revealed that wear rate is significantly influenced by wt.% ZrO_2, explaining 47.15% of the variability. Normal applied load followed by a contribution of 36.04%, slide distance of 13.51%, and an error term of 3.30%.

ANOVA indicated that normal applied load had a substantial impact on the friction factor, explaining 39.02% of the variability. Sliding distance followed with a contribution of 29.73%, wt.% of ZrO_2 with 19.04%, and an error term of 12.21%.

The analysis reveals that specific wear is primarily influenced by normal applied load, which contributes 47.06% to the variation. Sliding distance contributes 23.53%, while wt.% of ZrO_2 accounts for 17.63%. The error term represents 11.76% of the total variation.

The R^2 values for wear rate, friction factor, and specific wear are 84.58%, 87.79%, and 81.51%, respectively, indicating a strong fit of the models to the experimental data.

According to the SEM analysis, AlZ6 with 6 wt.% ZrO_2 exhibited the best wear resistance due to its optimal balance of hardness and toughness, resulting in smoother surfaces and reduced debris formation. In contrast, AlZ9 with 9 wt.% ZrO_2 displayed increased abrasive and delamination wear due to its brittle behavior and high ZrO_2 content.

FUNDING

This research received no specific grant from any funding agency in the public, commercial, or not-for-profit sectors.

CONFLICTS OF INTEREST

The authors declare that there is no conflict of interest.

COPYRIGHT

This article is an open-access article distributed under the terms and conditions of the Creative Commons Attribution (CC BY) license (http://creativecommons.org/licenses/by/4.0/).

REFERENCES

Babu, R. R., Rajendran, C., Saiyathibrahim, A. and Velu, R., Influence of B4C and ZrB2 reinforcements on microstructural, mechanical and wear behaviour of AA 2014 aluminium matrix hybrid composites, *Def. Technol.,* 40, 242–254(2024). https://doi.org/10.1016/j.dt.2024.05.009

Bennett, S. K., Velmurugan, K. V., Rajendiran, M., Srimathy, G., Devi, D. C., Bohidar, S. K. and Velumayil, R., Optimization of sintering parameters in aluminium metal matrix composites via Taguchi method and ANOVA analysis, *AIP Conf. Proc*, 3270(1), 20247(2025). https://doi.org/10.1063/5.0270427

Gajević, S., Miladinović, S., Güler, O., Özkaya, S. and Stojanović, B., Optimization of dry sliding wear in hot-pressed Al/B4C metal matrix composites using Taguchi method and ANN, *Mater*., 17(16), 4056(2024). https://doi.org/10.3390/ma17164056

Geng, R., Qiu, F. and Jiang, Q., Reinforcement in Al Matrix Composites: A Review of Strengthening Behavior of Nano-Sized Particles, *Adv. Eng. Mater.*, 20(9), 1701089(2018). https://doi.org/10.1002/adem.201701089

Haja, P. S. M., Jayakumar, V., Bharathiraja, G. and Palani, K., Investigations on mechanical and wear behaviour of graphene and zirconia reinforced AA6061 hybrid nanocomposites using ANN and Sugeno-type fuzzy inference systems, *Mater. Res. Express.*, 9(11), 115002(2022). https://doi.org/10.1088/2053-1591/ac9c86

Kar, A., Sharma, A. and Kumar, S., A Critical Review on Recent Advancements in Aluminium-Based Metal Matrix Composites. *Cryst.*, 14(5), 412(2024). https://doi.org/10.3390/cryst14050412

Keshavarz, H., Moosavi, S. E., Eslamian, H. and Kokabi, A., Corrosion behavior and tribological-microstructural characterization of Al/ZrO_2-Gr hybrid composite fabricated via Friction Stir Processing, *J. Alloys Compd.*, 960, 170770(2023). https://doi.org/10.1016/j.jallcom.2023.170770

Khazin, M. L., Apakashev, R. A. and Davydov, S. Y., Obtaining Aluminum –Matrix Composite Materials Particulate-Reinforced with Ceramic Particles, *Refract. Ind. Ceram.*, 63(3), 291–296(2022). https://doi.org/10.1007/s11148-022-00719-4

Kumar, N. and Irfan, G., A review on tribological behaviour and mechanical properties of Al/ZrO_2 metal matrix nano composites, *Mater. Today. Proc.,* 38, 2649–2657(2021). https://doi.org/10.1016/j.matpr.2020.08.240

Manghnani, S., Shekhawat, D., Goswami, C., Patnaik, T. K. and Singh, T., Mechanical and tribological characteristics of Si3N4 reinforced aluminium matrix composites: A short review. *Mater. Today. Proc.*, 44, 4059–4064(2021). https://doi.org/10.1016/j.matpr.2020.10.440

Manikandan, S. P., Vetrivel, K. P., Thakre, P., Swarnalatha, K., P, N. and Chandrasekar, G., Artificial Neural Network and Taguchi Analysis of Multi-Objective Optimisation of Wear Behaviour of ZrO_2 based Aluminium Nanocomposite. 2023 Second International Conference on Electronics and Renewable Systems (ICEARS), 416–421(2023). https://doi.org/10.1109/icears56392.2023.10084968

Messer, O., Ratzker, B., Shilo, J. T., Kalabukhov, S. and Sokol, M., The effect of coarse and fine Ti3SiC2 particle reinforcement in aluminum matrix composites, *J. Alloys Compd.*, 976, 173150(2024). https://doi.org/10.1016/j.jallcom.2023.173150

Mu, D. K. Q., Zhang, Z., Xie, Y. H., Liang, J. M., Wang, J. and Zhang, D. L., The microstructures and mechanical properties of a 5vol%SiC/AA2024 nanocomposite fabricated by powder metallurgy, *Mater. Charact.,* 175, 111090(2021). https://doi.org/10.1016/j.matchar.2021.111090

Nie, Z., Lu, H., Yang, F. and Xu, G., Preparation and property enhancement of SiC particle-reinforced aluminum matrix composites based on Micro-arc Oxidation, *J. Alloys. Compd.*, 1010, 177388(2025). https://doi.org/10.1016/j.jallcom.2024.177388

Pal, K., Navin, K. and Kurchania, R., Study of structural and mechanical behaviour of Al-ZrO_2 metal matrix nanocomposites prepared by powder metallurgy method, *Mater. Today. Proc.*, 26, 2714–2719(2020). https://doi.org/10.1016/j.matpr.2020.02.570

Pooja, K., Tarannum, N. and Chaudhary, P., Metal matrix composites: revolutionary materials for shaping the future, *Discover. Mater.,* 5(1), 35(2025). https://doi.org/10.1007/s43939-025-00226-6

Prakash, P. P., Kumar, S. R. and Chauhan, P. S., Analysis and investigation of the efficacy of the nanoparticles on the mechanical properties of aluminium metal matrix composites, A review, *Mater. Today. Proc.,* 103, 76–80(2024). https://doi.org/10.1016/j.matpr.2023.08.122

Rafiei, J. and Ghasemi, A. R., Development of thermo-mechanical simulation of WC/Inconel 625 metal matrix composites laser cladding and optimization of process parameters, *Int. J. Therm. Sci.,* 198, 108883(2024). https://dx.doi.org/10.1016/j.ijthermalsci.2024.108883

Ramesh, B. T., Giri, J., Al-Sadoon, M. K., Bongale, A. K., Sathish, T., Banagar, A. R. and others., Optimizing process parameters to minimize wear-induced material loss in bronze-based hybrid metal matrix composites using the Taguchi method, *AIP Adv.,* 14(9), 095104(2024). https://doi.org/10.1063/5.0203081

Sabari, K., Muniappan, A., Deepanraj, B. and Jinnah, S. M. M., Advanced Mechanical Performance Optimization of Friction Stir Welded AZ31 Magnesium Alloy Using Artificial Neural Network and Grey Relational Analysis, *Surf. Rev. Lett.,* 2550117(2024). https://doi.org/10.1142/s0218625x25501173

Sabari, K., Muniappan, A., Deepanraj, B. and Mohamed, M. J. S., Enhancing Mechanical Performance of Friction Stir Welded AZ31 Magnesium Alloy with Nano-TiC Reinforcements Using Grey Relational Analysis, *Int. J. Precis. Eng. Manuf.*, 29, e2914(2024). https://doi.org/10.1590/0104-9224/SI29.14

Sabbar, H. M., Leman, Z., Shamsudin, S. B., Tahir, S. M., Aiza, J. C. N., Hanim, M. A. A., Ismsrrubie, Z. N. and Al-Alimi, S., AA7075-ZrO_2 Nanocomposites Produced by the Consecutive Solid-State Process: A Review of Characterisation and Potential Applications, *Met.,* 11(5), 805(2021). https://doi.org/10.3390/met11050805

Sahoo, S., Jha, B. B. and Mantry, S., Optimization of process parameters of hot consolidated steel matrix composites by Taguchi method, *JOM.*, 76(2), 818–828(2024). http://ore.immt.res.in/handle/2018/3446

Said, Z., Pandey, A. K., Tiwari, A. K., Kalidasan, B., Jamil, F., Thakur, A. K., Tyagi, V. V, Sarı, A. and Ali, H. M., Nano-enhanced phase change materials: Fundamentals and applications. Progress in Energy and Combustion Science, 104, 101162(2024). https://doi.org/https://doi.org/10.1016/j.pecs.2024.101162

Şenel, M. C., Gürbüz, M. and Koç, E., Fabrication and characterization of aluminum hybrid composites reinforced with silicon nitride/graphene nanoplatelet binary particles. *J. Compos. Mater.*, 53(28–30), 4043–4054(2019). https://doi.org/10.1177/0021998319853329

Sharma, A. K., Bhandari, R. and Pinca-Bretotean, C., A systematic overview on fabrication aspects and methods of aluminum metal matrix composites, *Mater. Today. Proc.*, 45, 4133–4138(2021). https://doi.org/https://doi.org/10.1016/j.matpr.2020.11.899

Singh, M., Bhandari, D. and Goyal, K., A review of the mechanical performance of nanoparticles reinforced aluminium matrix nanocomposites, *Mater. Today. Proc*., 46, 3198–3204(2021). https://doi.org/10.1016/j.matpr.2020.11.191

Singhal, V., Shelly, D., Saxena, A., Gupta, R., Verma, V. K. and Jain, A., Study of the Influence of Nanoparticle Reinforcement on the Mechanical and Tribological Performance of Aluminum Matrix Composites, A Review, *Lubr.*, 13(2), 93(2025). https://doi.org/10.3390/lubricants13020093

Taha, M. A., Zawrah, M. F. and Abomostafa, H. M., Fabrication of Al/Al2O3/ SiC/graphene hybrid nanocomposites from Al-dross by powder metallurgy: Sinterability, mechanical and electrical properties, *Ceram. Int.*, 48(14), 20923–20932(2022). https://doi.org/10.1016/j.ceramint.2022.04.084

Tran, D., Lin, C. K., Tung, P. C., Ho, J. R. and Le, T. L., Enhancing mechanical properties of selective-laser-melting TiN/AISI 420 composites through Taguchi GRA and PCA multi-response optimization, *J. Mater. Res. Technol.*, 29, 1278–1292(2024). https://doi.org/10.1016/j.jmrt.2024.01.174

Vignesh, M., Anbuchezhiyan, G., Mamidi, V. K. and Vivek, A. A., Enriching mechanical, wear and corrosion behaviour of SiO2/TiO2 reinforced Al 5754 alloy hybrid composites, *Mater. Lett.*, 361, 136106(2024). https://doi.org/10.1016/j.matlet.2024.136106

Vinoth, B., Alagarsamy, S. V., Meignanamoorthy, M., Ravichandran, M., Prediction of tribological performance of AA8011/wt.%ZrO2 based composites fabricated by stir casting route. Proceedings of the Institution of Mechanical Engineers, Part E: *J. Process. Mech. Eng.*, 236(6), 2420–2433(2022). https://doi.org/10.1177/09544089221096096

Wang, Z., Zhou, M., Jiang, Y., Sui, Y. and Li, Z., Impact-abrasive wear property of ZrO_2 toughened Al2O3 ceramic particles reinforced high manganese steel matrix composites, *Tribol. Int.*, 194, 109547(2024). https://doi.org/10.1016/j.triboint.2024.109547

Wu, D., Zhang, J., Li, W., Xu, Y., Yang, X. and Su, Y., Morphology of ceramic regulates the deposition behavior and mechanical properties of cold spray additive manufactured Al2O3/2024 aluminum matrix composites, *Mater. Charact.*, 215, 114197(2024). https://doi.org/10.1016/j.matchar.2024.114197